Location of Substrate Binding Sites within the Integral Membrane Protein Microsomal Glutathione Transferase-1†

Laura S. Busenlehner,‡ Johan Ålander,§ Caroline Jegerscöhld,|| Peter J. Holm,||,⊥ Priyaranjan Bhakat,|| Hans Hebert,|| Ralf Morgenstern,§ and Richard N. Armstrong*,‡

Departments of Biochemistry and Chemistry, Center in Molecular Toxicology, Vanderbilt University School of Medicine, Nashville, Tennessee 37232-0146, Institute of Environmental Medicine, Division of Biochemical Toxicology, Karolinska Institutet, SE-17177 Stockholm, Sweden, and Department of Biosciences and Nutrition, Karolinska Institutet, and School of Technology and Health, Royal Institute of Technology, SE-14157 Huddinge, Sweden

Received November 13, 2006; Revised Manuscript Received December 20, 2006

ABSTRACT: Microsomal glutathione transferase-1 (MGST1) is a trimeric, membrane-bound enzyme with both glutathione (GSH) transferase and hydroperoxidase activities. As a member of the MAPEG superfamily, MGST1 aids in the detoxication of numerous xenobiotic substrates and in cellular protection from oxidative stress through the GSH-dependent reduction of phospholipid hydroperoxides. However, little is known about the location of the different substrate binding sites, including whether the transferase and peroxidase activities overlap structurally. Although molecular density attributed to GSH has been observed in the 3.2 Å resolution electron crystallographic structure of MGST1, the electrophilic and phospholipid hydroperoxide substrate binding sites remain elusive. Amide H−D exchange kinetics and H−D ligand footprinting experiments indicate that GSH and hydrophobic substrates bind within similar, but distinct, regions of MGST1. Site-directed mutagenesis, guided by the H−D exchange results, demonstrates that specific residues within the GSH footprint effect transferase activity toward 1-chloro-2,4-dinitrobenzene. In addition, cytosolic residues surrounding the chemical stress sensor C49 but not modeled in the crystal structure appear to play an important role in the formation of the binding site for hydrophobic substrates. Although the fatty acid/phospholipid binding site structurally overlaps that for GSH, it does not appear to be localized to the same region as other hydrophobic substrates. Finally, H−D exchange mass spectrometry reveals a specific conformational transition that may mediate substrate binding and/or product release. Such structural changes in MGST1 are essential for activation of the enzyme and are important for its biological function.

Reactive chemical intermediates trigger intracellular damage by covalent binding to or modification of endogenous targets. This can result in impaired cellular function, genotoxicity, and cancer. Glutathione transferases (EC 2.5.1.18) are important enzymes involved in Phase II detoxication of numerous carcinogenic, mutagenic, and pharmacologically active substances by conjugation of the tripeptide glutathione (GSH)[1] to these electrophilic compounds. Glutathione transferases have diverse substrate specificities and include both cytosolic and membrane-bound proteins. The membrane-bound enzymes are not structurally related to cytosolic GSH transferases but are part of the MAPEG superfamily, membrane-associated proteins in eicosanoid and glutathione metabolism (Figure 1). The MAPEG family includes microsomal glutathione transferase-1 (MGST1), MGST2, MGST3, microsomal prostaglandin E_2 synthase-1 (MPGES1), leukotriene C_4 synthase (LTC4S), and 5-lipoxygenase activating protein (FLAP) (*1*, *2*). This enzyme superfamily is involved in metabolism of xenobiotics such as chemotherapeutic drugs (*3*) and in the biosynthesis of mediators of fever, inflammation, pain, allergy, and asthma (*1*, *2*).

One of the more studied members of the MAPEG superfamily, MGST1, has both glutathione transferase and hydroperoxidase activities. As a glutathione transferase, MGST1 exhibits selectivity for halogenated arenes such as 1-chloro-2,4-dinitrobenzene (CDNB), as well as polyhalogenated unsaturated hydrocarbons (*4*). The GSH-dependent peroxidase activity of MGST1 protects membranes from oxidative modification through the reduction of phospholipid and fatty acid hydroperoxides (*5*, *6*). Due to these specific activities, MGST1 contains three types of substrate binding sites: a GSH binding site, a hydrophobic substrate site, and a fatty acid/phospholipid substrate binding site. Recently, a 3.2 Å resolution electron crystallographic structural model

† Supported by Grants R01 GM30910, P30 ES00267, T32 ES07028, and F32 ES13105 from the National Institutes of Health, the Swedish Cancer Society, the Swedish National Board for Laboratory Animals, funds from the Karolinska Institutet, and Swedish Research Council Grants 00144 and 621/3056.

* To whom correspondence should be addressed. E-mail: r.armstrong@vanderbilt.edu. Telephone: (615) 343-2921. Fax: (615) 343-2920.

‡ Vanderbilt University School of Medicine.

§ Division of Biochemical Toxicology, Karolinska Institutet.

|| Department of Biosciences and Nutrition, Karolinska Institutet, and Royal Institute of Technology.

⊥ Present address: HØIBERG A/S, St. Kongensgade 59 A, 1264 Copenhagen K, Denmark.

[1] Abbreviations: MGST1, microsomal glutathione transferase-1; GSH, glutathione; CDNB, 1-chloro-2,4-dinitrobenzene; IPTG, isopropyl *β*-D-thiogalactopyranoside; GSO_3^-, glutathione sulfonate; GSDNB, 1-(*S*-glutathionyl)-2,4-dinitrobenzene; LTC4, leukotriene C4; H−D, hydrogen−deuterium; GS^-, glutathione thiolate anion.

10.1021/bi6023385 CCC: $37.00
Published on Web 02/13/2007

FIGURE 1: Sequence alignment of MAPEG family members. The multiple-sequence alignment for rat (this study), pig, and human MGST1 homologues, human MPGES1, human MGST2, human MGST3, human LTC4S, and human FLAP was generated with ClustalW (*45*). The helices for rat MGST1 are indicated above the sequences and are based on the three-dimensional structural model. Conserved residues are marked with an asterisk, while highly and moderately conserved residues are marked with and a colon and a period, respectively.

of MGST1 with GSH bound was reported (*7*). This is the first atomic-level structural information for any MAPEG protein.

One interesting property of MGST1 is that the enzyme functions as an intracellular, chemical stress sensor and is activated up to 30-fold by modification of a single cysteine residue (C49) by alkylating agents, oxidation, and other treatments (*8*−*11*). As an adaptive response to cells undergoing oxidative or chemical stress (*12*, *13*), modification of the C49 stress sensor increases the efficiency of a rate-limiting conformational transition upon binding of GSH (*11*−*14*). Amide hydrogen−deuterium (H−D) exchange studies indicated that this conformational transition involves the rearrangement of two transmembrane helices (α1 and α3) and portions of the cytosolic domain in forming a more favorable conformation for GSH binding and ionization (*13*).

Inasmuch as global decreases in the kinetics of amide H−D exchange were observed upon addition of GSH to MGST1, the regions directly involved in GSH binding were localized to the cytosol-facing side of the enzyme (*13*). This is consistent with the three-dimensional, electron crystallographic structure of trimeric MGST1 in which additional cytosolic molecular density in the map is attributed to the presence of GSH (*7*). The locations of the hydrophobic and fatty acid/phospholipid binding sites have yet to be elucidated. Biochemical experiments indicated that the electrophilic substrate site, which binds xenobiotics and other active compounds such as CDNB, also faces the cytosolic side of the membrane (*15*). The fatty acid/phospholipid binding site was suggested to be distinct from the electrophilic substrate site on the basis of the fact that the fatty acid derivative leukotriene C_4 (LTC_4) is a noncompetitive inhibitor toward the electrophilic substrate CDNB (*16*). LTC_4 is the glutathione conjugate of LTA_4, a metabolite of arachidonic acid, that binds with high affinity to MGST1 with a stoichiometry of one LTC_4 per trimer (*16*, *17*). LTC_4 synthase, the MAPEG enzyme responsible for the addition of GSH to LTA_4, interacts with MGST1 in vivo and in vitro, indicating that MGST1 might serve as a storage protein for LTC_4 or that LTC_4 may regulate the phospholipid/fatty acid peroxidase activity (*18*−*20*).

In this report, we describe the use of amide hydrogen−deuterium exchange monitored by mass spectrometry to investigate the locations of the MGST1 binding sites for GSH, electrophilic, and fatty acid/phospholipid substrates, as well as to map conformational changes that may occur upon binding of substrate and product ligands (Figure 2). Amide H−D exchange experiments monitoring incorporation of deuterium into the backbone of MGST1 as a function of time revealed a specific GSH/GSO_3^--dependent conformational transition involving two transmembrane helices that cannot be reproduced by product GSDNB or LTC_4. This transition may reflect local changes in MGST1 structure controlling substrate binding and product release. In addition, ligand protection assays (H−D footprinting) illuminate specific regions that are protected by GSH and hydrophobic substrates. These results, along with site-directed mutagenesis, provide experimental evidence to support a structural model for binding of GSH and indicate that a region of the protein not observed in the crystal structure participates in

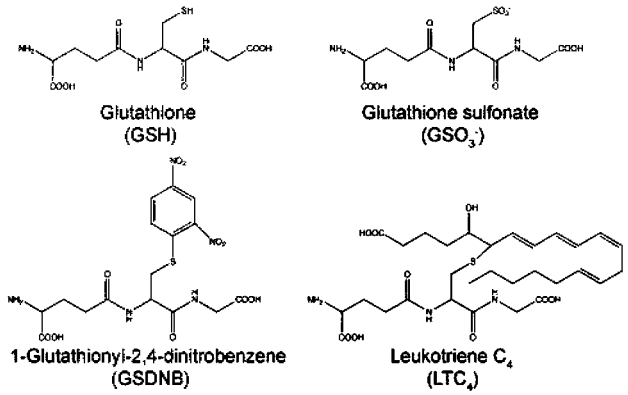

FIGURE 2: Chemical structures of glutathione, glutathione sulfonate, 1-glutathionyl-2,4-dinitrobenzene, and leukotriene C_4.

binding electrophilic substrates. This is the first indication of the location of cosubstrate binding sites in any MAPEG protein.

EXPERIMENTAL PROCEDURES

Materials. Deuterium oxide (99.9 at. % D), reduced glutathione, glutathione sulfonate, 1-chloro-2,4-dinitrobenzene, and porcine pepsin were purchased from Sigma Chemical Co. (St. Louis, MO). Leukotriene C_4 was obtained from Cayman Chemical (Ann Arbor, MI).

Purification of the Wild-Type Enzyme. Wild-type MGST1 was isolated and purified from male Sprague-Dawley rat livers as previously described (*21*). The protein was stored in 10 mM potassium phosphate (pH 7.0), 0.1 M KCl, 0.1 mM EDTA, 1 mM glutathione, 0.2% Triton X-100, and 20% glycerol. GSH was removed prior to mass spectrometry (*13*). Stock protein samples for H−D exchange experiments (98 μM; 1.7 mg/mL monomeric MGST1) were aliquoted, purged with N_2 gas, and flash-frozen at −80 °C.

Site-Directed Mutagenesis. The plasmid *p*SP19T7LTrμGT, containing wild-type rat MGST1, was used as the template for site-directed mutagenesis (*22*). The forward primers used for the mutagenesis are listed in Table 1. Mutated plasmids were transformed into *Escherichia coli* XL1-blue, grown overnight at 37 °C in LB medium, and pelleted by centrifugation. Plasmids were then purified, sequenced, and transformed into *E. coli* BL21(DE3)*p*LysSL for protein expression.

Expression and Purification of Mutant MGST1. A small aliquot of the *E. coli* BL21(DE3)*p*LysSL glycerol stock was added to 3 mL of 2× YT medium and incubated overnight at 37 °C. The culture was diluted 1:100 in Terrific Broth and grown until the OD_{600} was 0.4−1.2. At this point, protein expression was induced with 1 mM IPTG overnight at 30 °C. All cell cultures contained ampicillin (75 μg/mL) and chloramphenicol (10 μg/mL). After expression, cells were pelleted at 4000*g* for 10 min and resuspended in 10 mL of 15 mM Tris-HCl (pH 8.0), 0.25 M sucrose, 0.1 mM EDTA, and 1 mM glutathione per 100 mL of bacterial culture. The cells were subsequently lysed by sonication using four 30 s pulses. Cell debris was removed by centrifugation at 5000*g* for 10 min, and the supernatant was centrifuged at 184000*g* for 2 h to pellet the membrane fraction. The membrane pellet was resuspended in 2 mL of buffer A [10 mM potassium phosphate (pH 7.0), 20% glycerol, 0.1 mM EDTA, and 1 mM GSH] and homogenized.

Determination of Protein Concentration. The total protein concentration was measured by the method of Peterson using bovine serum albumin as the standard (*23*). The MGST1 concentration in membrane fractions was determined through Western blotting with polyclonal antibodies against full-length MGST1. Bands were detected using the ECL Western Blotting Detection Reagent (Amersham Biosciences) and quantified using Scion Image (http://www.scioncorp.com). Purified MGST1 was used as the standard.

Enzyme Activity Assay. Specific enzyme activity in homogenized membrane fractions was assayed with CDNB (0.5 mM) and GSH (5 mM) at 340 nm ($\epsilon = 9600\ M^{-1}\ cm^{-1}$) in 0.1 M potassium phosphate, 0.1 M Tris-HCl, and 1% Triton X-100 at pH 6.5 and 30 °C, essentially as described previously (*24*). Activities are expressed as a percentage of that of the wild type ± the standard error of mean (SEM). Due to turbidity, a maximum of 5 μL of the membrane fraction per 100 μL final reaction volume was used for activity measurements.

Synthesis of 1-(S-Glutathionyl)-2,4-dinitrobenzene (GSDNB). GSDNB was synthesized and purified according to the combined methods of Chang et al. (*25*) and Hinchman et al. (*26*). CDNB (3 mmol) was dissolved in 8 mL of a 50% ethanol/H_2O mixture. Glutathione (2.5 mmol) was added to the CDNB solution over a period of 1.5 h while the pH was continually maintained at 7.0−8.0 with 0.2 N potassium hydroxide. The product, GSDNB, was insoluble under these conditions. The ethanol was evaporated by bubbling argon gas, and the unreacted CDNB was subsequently removed by four ethyl ether extractions. The remaining solution was acidified to pH 2.0 with dilute hydrochloric acid. The precipitate was washed with cold H_2O and collected by vacuum filtration. The product was recrystallized on ice after the precipitate had been dissolved with boiling water and vacuum filtered to dryness. The purity of GSDNB was determined via electrospray mass spectrometry, UV−visible spectroscopy, and HPLC analysis, as described previously (*25*).

Table 1: Forward Primers Used To Construct MGST1 Mutations[a]

mutation	primer sequence
S30A	5′ GCCAAGATGATGTTCCTGGCCTCCGCGACTGCATTCCAG 3′
R63A	5′ GAATGCCAAGAAGTTCCTTGCGACTGACGAGAAGGTGGAAC 3′
T64V	5′ GCCAAGAAGTTCCTTCGGGTTGACGAGAAGGTGGAACGC 3′
R72A	5′ GAAGGTGGAACGCGTGGCAAGAGCCCACCTGAATG 3′
R73Q	5′ GGAACGCGTGCGACAAGCCCACCTGAATGACC 3′
N77T	5′ CGAAGAGCCCACCTGACTGACCTTGAAAACATCG 3′
E80Q	5′ CCTGAATGACCTTCAAAACATCGTTCCCTTTTCTCG 3′
R113K	5′ CTTTGTGGGCGCTAAGATCTACCACACCATTGC 3′

[a] The codons to be mutated are underlined.

Amide Hydrogen−Deuterium Exchange Mass Spectrometry. Amide H−D exchange experiments were carried out with GSH, the inhibitor glutathione sulfonate (GSO_3^-), the product (GSDNB), and the fatty acid derivative leukotriene C_4 (LTC_4). Complexes of MGST1 with GSH, GSO_3^-, and GSDNB were prepared by the addition of 3 mM ligand [10 mM potassium phosphate (pH 7.0)] to 1.7 mg/mL apoMGST1. The complex of MGST1 and LTC_4 was formed by the addition of LTC_4 (100 μM in water) to 1.0 mg/mL apoMGST1 to form the MGST1·LTC_4 complex. All MGST1 H−D exchange samples were prepared individually and run on the same day.

Deuterium in-exchange was initiated by the addition of 40 μL of D_2O to 10 μL of each MGST1 complex and incubated for 15 s to 6 h at 23 °C. In-exchange was quenched by acidification with 50 μL of cold quench buffer (0.1 M potassium phosphate at pH 2.3 in H_2O at 0 °C) followed by immediate transfer to ice. Digestion was initiated by 1.5 equiv (w/w) of pepsin (5 μL of a 5 mg/mL solution in H_2O) and allowed to proceed on ice for 5 min. Deuterium control experiments for determining the amount of artifactual exchange of deuterium that occurred after the acidification and during the digest ($m_{0\%}$) and the loss of deuterium during HPLC chromatography ($m_{100\%}$) were performed as described previously (*13*, *27*).

The amino acid sequences of peptides generated from the pepsin digest have previously been identified using tandem mass spectrometry (*13*). The HPLC-based separation of identified MGST1 peptic peptides has been reported in detail and was utilized without alteration (*13*). Mass spectra were recorded on a ThermoFinnigan TSQ Quantum triple-quadrupole mass spectrometer using positive ion electrospray ionization (*13*). H−D exchange data were collected with a scan time of 1 s and a peak width of 0.7 by scanning from *m*/*z* 300 to 1500.

Kinetic Analysis. Finnigan Xcalibur software was utilized to locate individual peptide ions. Individual scans within the extracted chromatographic ion profile for each peptide were averaged to produce the composite spectrum, and the centroid of the spectrum at each deuterium time point (m_t) was calculated using MagTran 1.0 beta 9 (*28*). The incorporation of deuterium into each peptide was corrected for the gain ($m_{0\%}$) and loss ($m_{100\%}$) of deuterium during analysis by the following expression (*29*):

$$D_t = N\left(\frac{m_t - m_{0\%}}{m_{100\%} - m_{0\%}}\right) \quad (1)$$

where D_t is the corrected level of deuterium incorporation of a peptide at time t and N is the total number of exchangeable amide protons (less one for the N-terminal amide proton and any proline residues). The level of incorporation of deuterium into each peptide was plotted as a function of time, and the progress curves were fit to the sum of first-order rate expressions given by eq 2 (*13*, *27*):

$$D = N - A_1 e^{-k_1 t} - A_2 e^{-k_2 t} - A_3 e^{-k_3 t} \quad (2)$$

where D is the number of deuterium atoms incorporated, N is the total number of exchangeable amide protons, and A_n is the amplitude or number of amide protons exchanging with a give rate constant, k_n. Progress curves were fit to either a single- or double-exponential equation as appropriate on the basis of the goodness of fit.

Ligand Footprinting Experiments with H−D Exchange. A different application of H−D exchange called footprinting was employed to provide support for the identification of the ligand binding sites (*30*, *31*). In these experiments, surface amides in apoMGST1 are "on-exchanged" with deuterons (15 min incubation in D_2O). Next, ligand is added at the concentration that saturates the binding site and is allowed to equilibrate (5 min). Those amide deuterons protected by ligand at the binding interface become trapped. After "off-exchanging" deuterium by diluting it into H_2O (15 s or 10 min), protected amide sites retain deuterium. These regions are localized through pepsin digestion and quantified using mass spectrometry. For footprinting experiments, apoMGST1 was concentrated to 5.0 mg/mL (294 μM) prior to use. Stock solutions of GSH (750 mM), GSO_3^- (750 mM), and GSDNB (500 mM) were prepared in 0.1 M ammonium acetate (in D_2O) at pD 7.0. The concentration of the LTC_4 stock solution was 3 mM (10 mM potassium phosphate in H_2O at pH 6.5). Pepsin digestion, HPLC analysis, and mass spectrometry for footprinting experiments follow the same procedure as the H−D exchange kinetic experiments.

To determine the total deuterium content for apoMGST1 during the exchange period, apoMGST1 (5 μL of a 5.0 mg/mL solution) was incubated with 45 μL of D_2O for 20 min, quenched by acidification to pH 2.3 (450 mL of ice-cold H_2O with 0.15% formic acid), and then digested with 1.5 equiv of pepsin [~3 μL of a 25 mg/mL solution in 10 mM potassium phosphate (pH 7.0)]. The loss of the deuterium label from apoMGST1 during off-exchange in H_2O was assessed by incubation in D_2O for 20 min as before, after which the sample was immediately diluted with 450 μL of H_2O for either 15 s or 10 min. The off-exchange was then quenched with cold, 0.15% formic acid (10 μL of a 7.5% solution), and the sample was transferred to ice prior to pepsin digestion.

To trap the deuterium label at each ligand binding site, thus creating the H−D footprint, three samples of apoMGST1 were incubated for 15 min in D_2O, followed by addition of ligand (30 mM GSH, 30 mM GSO_3^-, 10 mM GSDNB, or 0.35 mM LTC_4) and equilibrated for 5 min (20 min total D_2O exposure). One sample was not off-exchanged with H_2O after deuterium incorporation and served as the reference, while the other two were diluted into 450 mL of H_2O for 15 s or 10 min. All samples were quenched with 0.15% formic acid and digested with pepsin. Deuterium control experiments for determining the amount of artifactual exchange that occurred after the acidification and during the digest ($m_{0\%}$) and the loss of deuterium during HPLC ($m_{100\%}$) were performed essentially as described for kinetic experiments.

The number of deuterium atoms incorporated within each peptide was determined by the centroid method outlined for the H−D exchange kinetic experiments (eq 1). The control experiments with apoMGST1 or liganded MGST1 that were not off-exchanged with H_2O serve as the reference for each state and define the starting amount of deuterium in each peptide prior to off-exchange. For each off-exchanged time point, the amount of deuterium label retained by each peptide in the apoMGST1 samples that were off-exchanged with H_2O for 15 s and 10 min was subtracted from that retained in the ligand-bound MGST1 samples that were off-exchanged for

the equivalent length of time. These values are compared to those of the appropriate apo or ligand-bound 20 min D_2O incubation control with no off-exchange and are the average of three independent determinations.

RESULTS

Identification of Residues Involved in Thiolate Anion Stabilization in the GSH Site. Ligand binding sites can be successfully localized to proteins through ligand-induced alterations in the kinetics of backbone amide hydrogen−deuterium exchange (*27*, *32*). Changes in protein structure and dynamic motions as a result of binding ligands can also be determined and correlated with protein function. Previous experiments using amide H−D exchange mass spectrometry revealed that specific regions of MGST1 facing the cytosol exhibited perturbations in structure upon active site binding of GSH (*13*). The significant conformational changes that occur in the entire cytosolic domain and parts of two of the transmembrane helices obscure the location of the bound GSH. However, the results are consistent with an active site that faces the cytosol as modeled in the electron crystallographic structure (*7*).

The MGST1 trimer exhibits one-third-of-the-sites reactivity and can stabilize only one GSH thiolate (GS^-) per trimer, with the remaining two binding sites occupied by GSH with significantly lower affinity[2] (*14*, *33*, *34*). Glutathione sulfonate (Figure 2) is a known GSH analogue and inhibitor that can occupy all three binding sites on the MGST1 trimer.[2] At least one of the GSO_3^- molecules binds with an affinity similar to that of GS^- ($K_d^{GSO_3^-} = 8.6\ \mu M$, and $K_d^{GS^-} = 18\ \mu M$) (*33*). GSO_3^- does not have a free sulfhydryl but maintains a negative charge and can bind cytosolic glutathione transferases in a manner similar to that of GS^- (*35*, *36*).

For these reasons, GSO_3^- was used as a surrogate for GSH in amide H−D exchange experiments in an attempt to locate the GSH binding site, especially the region involved in the ionization and stabilization of the thiolate moiety. Typically, ligand binding results in a decreased level of incorporation of deuterium into the peptide backbone in regions directly involved in its coordination. This can be due to solvent protection by the ligand or limited dynamic fluctuations as a result of an increased number of hydrogen bonding interactions (*27*, *35*, *37*). Since GSO_3^- forms a thermodynamically tighter complex than GS^- and binds three per trimer and the sulfonate moiety (SO_3^-) is larger than the thiolate (S^-), one might expect that GSO_3^- should limit dynamic fluctuations near the GSH binding site to a greater extent than does GSH (*35*). This should aid in the identification of the GSH binding site for MGST1.

As expected, GSO_3^- bound at the active site of MGST1 is capable of producing the same global conformational changes as GSH, including the increased solvent accessibility of the α1 and α3 transmembrane helices (peptides 19−23 and 104−106, respectively) compared to apoMGST1 (Figure 3A,B). In fact, only two peptides (53−62 and 62−69) exhibited differences in the kinetic profiles when the MGST1·GSO_3^- and MGST1·GSH complexes were compared (Figure 3C,D). Interestingly, a decreased level of

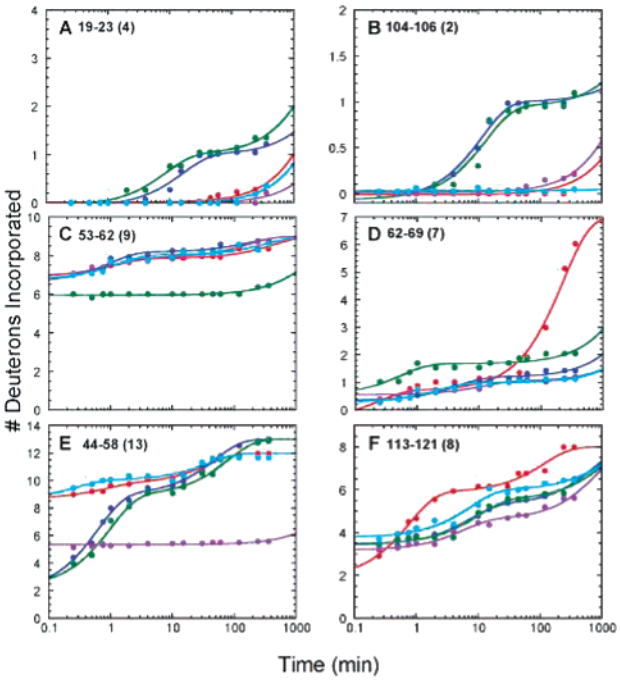

FIGURE 3: Amide H−D exchange kinetic profiles for MGST1. Shown are the average kinetic profiles for deuterium incorporation as a function of time for apoMGST1 and ligand-bound MGST1: apo (red), GSH (blue), GSO_3^- (green), GSDNB (purple), and LTC_4 (cyan). The solid lines are fits of the data to single- or double-exponential equations as described in Experimental Procedures (eq 2), with the fitted parameters supplied in Table S1 of the Supporting Information. The number in parentheses is the number of exchangeable amide protons for each peptide: (A) peptide 19−23, (B) peptide 104−106, (C) peptide 53−62, (D) peptide 62−69, (E) peptide 44−58, and (F) peptide 113−121. Data for apoMGST1 and the MGST1·GSH complex are from ref *13*.

deuterium incorporation is observed for residues 53−62 in the MGST1·GSO_3^- complex when compared to that in apoMGST1. This cytosolic region was not proposed to be involved in the binding of GSH since it did not exhibit changes in exchange kinetics with the substrate GSH (Figure 3C) (*13*). On the other hand, cytosolic peptide 62−69 displays a slight overall increase in the number of amide hydrogens exchanging for deuterium with the MGST1·GSO_3^- complex compared to that with the MGST1·GSH complex (Figure 3D). This result suggests that GSO_3^- does not shield amides within residues 62−69 from deuterium to the same extent as GSH. One explanation for the loss of ligand protection is that GSO_3^- may not interact with MGST1 in the same manner as the thiolate anion and is bound in an alternate conformation. In support of this hypothesis, the H−D exchange profiles for the adjacent peptide (53−62) that exhibit only GSO_3^--specific conformational changes suggest that this region is specifically involved in the binding of the analogue. Taken together, H−D exchange kinetics indicate that residues within peptide 62−69 are specifically involved in stabilizing GS^- while residues within peptide 53−62 participate in the binding of GSO_3^-.

Location of the GSH Binding Site by H−D Footprinting. Although H−D exchange experiments comparing the MGST1·GSH and MGST1·GSO_3^- complexes have implicated one protein segment that stabilizes GS^-, they have not conclusively identified other regions that compose the GSH binding site due to the similarity in H−D exchange kinetic profiles.

[2] J. Ålander and R. Morgenstern, unpublished observations.

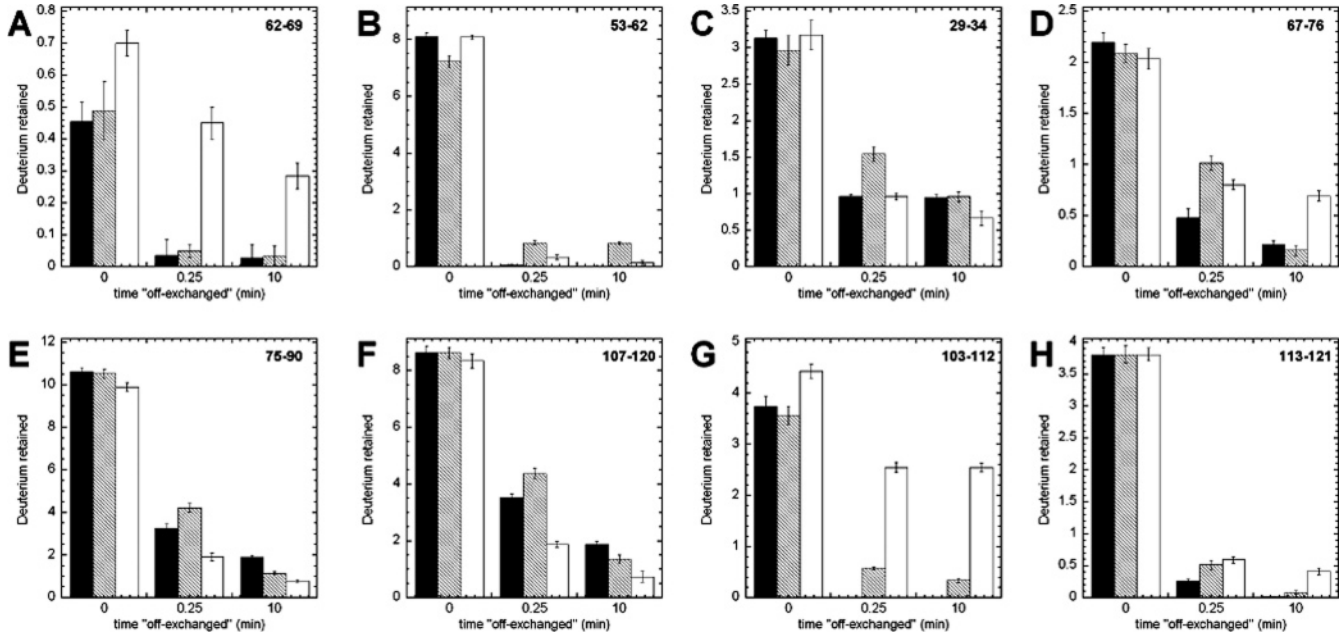

FIGURE 4: H−D exchange ligand footprinting experiments of MGST1 with GSH, GSO_3^-, and GSDNB. ApoMGST1 was incubated with D_2O for 15 min, the ligand added and equilibrated for 5 min, and then apoMGST1 either quenched with H_2O and formic acid (pH 2.3 and 0 °C) or off-exchanged with H_2O (pH 7 and 23 °C) for either 15 s or 10 min before quenching with formic acid. The amount of deuterium incorporated into each peptide after incubation in D_2O for 20 min serves as the reference (0 min off-exchange). The amount of deuterium remaining when apoMGST1 is off-exchanged with water for 15 s or 10 min is subtracted from the ligand-bound samples. The bar chart shows the average amount of deuterium retained or "trapped" by the ligand in each peptide as a function of time, with GSH (black), GSO_3^- (gray), and GSDNB (white): (A) peptide 62−69, (B) peptide 53−62, (C) peptide 29−34, (D) peptide 67−76, (E) peptide 75−90, (F) peptide 107−120, (G) peptide 103−112, and (H) peptide 113−121.

To more rigorously localize the GSH site, an alternate H−D exchange technique called H−D ligand footprinting was employed (*30*, *31*). This ligand protection assay involves incubating apoMGST1 with D_2O to exchange solvent-exposed amides for deuterium. After ligand (GSH, for example) is added, the protein complex is then diluted into H_2O to off-exchange the deuterium label. Those regions of MGST1 that are protected by ligand will retain more deuterium label compared to the apoprotein and can be quantified by mass spectrometry after pepsin digestion. Here, H−D footprinting experiments are described for both GSH and GSO_3^-.

The one peptide identified as part of the GSH site though H−D exchange kinetics, peptide 62−69, was of specific interest in H−D footprinting. Unfortunately, due to the low level of deuterium incorporation within this peptide after incubation for 20 min in D_2O (∼1 deuteron), the retention of deuterium label after off-exchange with GSH or GSO_3^- is too small to be conclusive (Figure 4A). If this peptide segment is involved in stabilizing only one thiolate anion per trimer, significant protection from off-exchange in this region may not be observed. However, the adjacent cytosolic peptide (53−62) implicated in stabilization of only GSO_3^- shows reproducible deuterium retention with GSO_3^- but not with GSH (Figure 4B). These results are consistent with H−D exchange kinetic experiments and clearly show that this region is directly influenced by the binding of GSO_3^-. Other regions that are protected by both GSO_3^- and GSH include peptides 29−34 in α1, 67−76 and 75−90 in α2, and 107−120 in α3 (Figure 4C−F). Of these peptides, all but peptide 75−90 were implicated through H−D exchange kinetic experiments in the binding of GSH (*13*).

Table 2: Specific Enzyme Activities of MGST1 Mutants

mutation	% of wild-type activity[a]
S30A	500 ± 80
R63A	130 ± 20
T64V	380 ± 60
R72A	42 ± 5
R73Q	57 ± 9
H75Q[b]	34
N77T[c]	ND[d]
E80Q[c]	7 ± 2
R113K[c]	5 ± 3

[a] From isolated *E. coli* membranes ($n = 3$). Values are expressed as the percentage of activity compared to the mean value of the specific activity of wild-type MGST1 for CDNB (5.6 ± 1.0 μmol min^{-1} mg^{-1}; $n = 11$). [b] From ref *24*. [c] Three separate protein expressions. [d] Not detectable.

In Vitro Mutagenesis. The H−D exchange kinetic and footprinting data were used in conjunction with the MGST1 structural model as a guide for site-specific mutations to functionally probe the GSH binding site. Amino acids within the footprint that are in the proximity of GSH based on the structural model were targeted first (R63A, R72A, R73Q, N77T, and E80Q). All of these mutations, with the exception of one mutation (R63A), result in a significant lowering of specific activity toward CDNB (Table 2). The R63A mutation has little effect on catalysis. Other mutations, more remote to the modeled GSH, include R113K, S30A, and T64V. Interestingly, the R113K mutant lost almost all activity. This is surprising since R113 is some distance from the GSH observed in the model at 3.2 Å resolution. Thus, it appears as though R113 may play a structural role, perhaps in organization of the GSH binding site through an intra-subunit hydrogen bonding network. Two additional amino

acid mutations, S30A and T64V, actually resulted in a substantial activation of MGST1. This result demonstrates that amino acids within the proposed footprint do have roles, perhaps in the dynamics of the GSH binding and thiolate formation. The structural model shows that S30 contacts Y137 from a neighboring subunit that when previously mutated (Y137F) also resulted in enzyme activation (*24*). Apparently, a structural link between S30 and Y137 mediates functional subunit interactions that influence the catalytic activity of the unactivated enzyme.

Prediction of the Electrophilic Substrate Binding Site. To date, there is little information about the exact location of the electrophilic substrate site in relation to the GSH binding site. To pinpoint specific segments of MGST1 involved in binding electrophilic xenobiotic substrates, amide H−D exchange kinetic experiments were performed with the GSH conjugate of CDNB, 1-(*S*-glutathionyl)-2,4-dinitrobenzene (Figure 2). The product GSDNB was used in place of the actual substrate CDNB since this compound may be able to activate MGST1 by alkylation of C49 at the long incubation times required for H−D exchange. In addition, CDNB is expected to have a weak affinity for MGST1 (*12*). Three GSDNB molecules are capable of binding to trimeric MGST1 ($K_d = 260\ \mu M$) and should presumably occupy both the GSH and hydrophobic sites.[2] A comparison of amide H−D exchange kinetic profiles for the MGST1·GSDNB and MGST1·GSH complexes should reveal areas comprising the binding site for hydrophobic substrates and may illuminate a product-specific conformation. The binding of product leads to global conformational changes similar to those with GSH, but GSDNB does not support the structural transition involving the α1 and α3 transmembrane helices observed for both GSH and GSO_3^- (Figure 3A,B). This indicates that this particular conformational transition is specific for the GSH-bound enzyme and is reversed after product formation at the active site, perhaps mediating substrate binding and product release.

Two additional peptides (44−58 and 113−121) show alterations in the H−D exchange kinetics of the MGST1·GSDNB complex that are not observed in the MGST1·GSH complex. The changes suggest that these regions are involved solely in binding hydrophobic substrates (Figure 3E,F). A significant change in the H−D exchange kinetic profile for peptide 44−58 occurs in the presence of GSDNB. This decrease in the level of deuterium incorporation indicates that this part of the cytosolic domain becomes more protected from solvent and experiences a reduction in dynamic motion, all consistent with ligand binding. This particular peptide includes the chemical stress sensor, C49, which can be modified by electrophilic reagents to activate the enzyme (*11*, *38*). Molecular density for this part of the cytosolic domain was observed in the electron crystallographic structure but could not be successfully modeled. Previous biochemical experiments indicate that C49 resides in a hydrophobic environment and that alkylation with *N*-ethylmaleimide might result in architectural or dynamic changes in the hydrophobic site. This rearrangement results in a higher-affinity binding site for CDNB (*12*). In addition to peptide 44−58, a small but reproducible decrease in the level of deuterium incorporation is observed in peptide 113−121 in the MGST1·GSDNB complex as compared to that of the MGST1·GSH complex. This peptide is located at the cytosolic (C-terminal) end of helix α3. When compared to apoMGST1, this region also experiences a change in solvent accessibility upon formation of the MGST1·GSH complex. However, the additional reduction in the level of deuterium incorporation in the MGST1·GSDNB complex can be attributed solely to contributions of the hydrophobic binding site.

Location of the Hydrophobic Site by H−D Footprinting. H−D exchange footprinting experiments with GSDNB revealed six peptides with more deuterium retention after off-exchange than with GSH (Figure 4). Three of these peptides (62−69, 103−112, and 113−121) exhibited significantly more protection of deuterated amides with GSDNB than with GSH or GSO_3^-, indicating participation in the hydrophobic binding site (Figure 4). Three additional peptides (29−34, 67−76, and 75−90) retained deuterium with either GSDNB or GSH/GSO_3^- bound. All three peptides (29−34, 67−76, and 75−90) are predicted to be involved in the binding of GSH from both H−D exchange kinetics and footprinting experiments. For peptides 29−34 and 75−90, the deuterated amides are protected in the MGST1·GSDNB complex, but the amount of deuterium retention is actually more pronounced in the MGST1·GSH complex (Figure 4C,E). This pattern indicates that these regions are involved in only the GSH binding site. In contrast, GSDNB maintains more deuterium label than GSH for peptide 67−76 after off-exchange for 10 min (Figure 4D). These data suggest that some structural overlap exists between the GSH and hydrophobic sites near residues 67−76, which may be functionally important. Although peptide 44−58 is predicted to be involved in the hydrophobic binding site, the signal-to-noise ratios for this peptide and several others were not sufficient for H−D exchange footprinting due to ion suppression of peptide signals by the high concentration of GSDNB (data not shown).

Taken together with the H−D exchange kinetic results, the hydrophobic substrate binding site of MGST1 appears to be formed, in part, by residues within peptides 44−58, 62−69, 67−76, 103−112, and 113−121. All of these peptides are predicted to reside within the cytosolic loops and the cytosolic-facing ends of transmembrane helices α2−α4. This analysis may not detect other regions involved in binding the electrophilic substrate, inasmuch as the experiments were performed with the product of the reaction and not the electrophilic substrate itself.

The Fatty Acid/Phospholipid Binding Site Overlaps the GSH Site. Leukotriene C_4 is a GSH adduct leukotriene A_4, a derivative of arachidonic acid, and is also considered a fatty acid analogue (Figure 2). MGST1 binds one molecule of LTC_4 per trimer ($K_d = 6$ nM) with significantly higher affinity than GSH. LTC_4 also inhibits GSH transferase activity (*16*, *17*). Reduction of fatty acid and phospholipid hydroperoxides is an important function of MGST1; however, little is known about the location of the fatty acid/phospholipid binding site. H−D exchange experiments with the MGST1·LTC_4 complex indicate that binding of the adduct induces conformational changes that mimic the binding of GSH with some notable exceptions. The specific conformational transitions involving helices α1 and α3, as well as those involving peptide 44−58 in the cytosolic domain and identified as part of the hydrophobic binding site, are not observed with the MGST1·LTC_4 complex

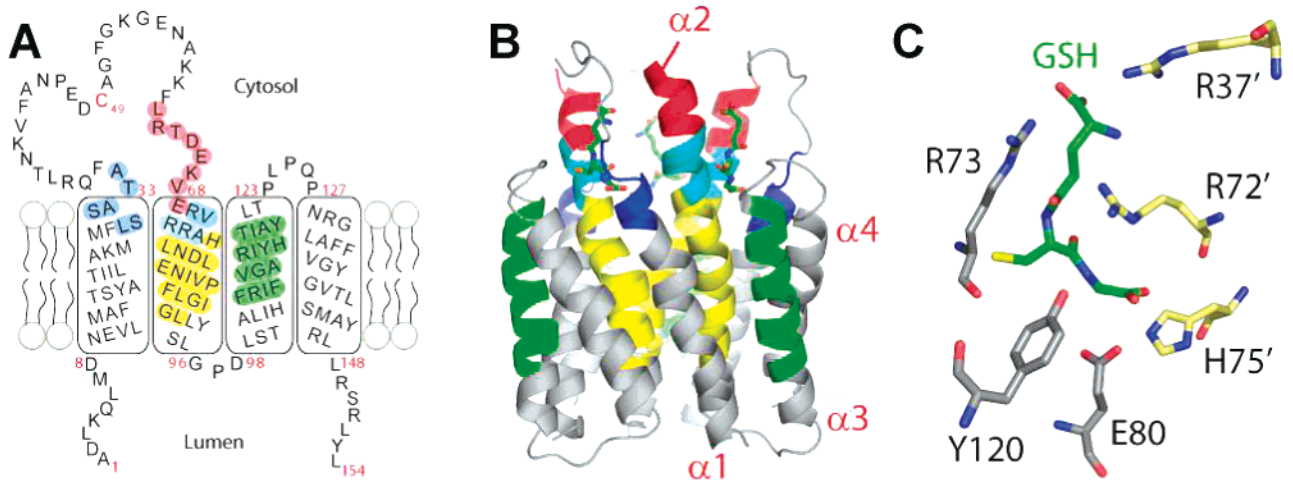

FIGURE 5: Regions influenced by the binding of GSH as indicated by amide H−D exchange kinetics and H−D footprinting with GSH and GSO_3^-. Peptides undergoing changes in H−D exchange are mapped to (A) the primary sequence with lipid-embedded helices and (B) the electron crystallographic model of trimeric MGST1 where the three observed GSH molecules are colored green (*7*). Peptides involved in GSH binding based on H−D exchange results are colored as follows: blue for 29−34, red for 62−69, yellow for 75−90, and green for 107−120. Residues from peptide 67−76 overlap other peptides; therefore, only residues 70−74 are colored cyan. (C) Residues involved in hydrogen bonding with GSH based on the crystallographic structural model are shown as sticks (*7*). This proposed GSH binding site is composed of R37′, R72′, and H75′ from one monomer (yellow backbone) and R73, E80, and Y120 from an adjacent monomer (gray backbone). The fatty acid/phospholipid binding site (not indicated) is predicted to overlap the GSH site.

(Figure 3A,B,E). It would appear that the fatty acid and glutathione binding sites are located within the same region of MGST1 but are distinct from the hydrophobic substrate site.

It is possible that there are other regions of the protein involved in fatty acid/phospholipid binding that cannot be observed by this technique. The long, hydrophobic tails of fatty acids and phospholipids may insert into the predicted central cavity in the transmembrane region (*7*) without inducing a change in deuterium incorporation since these solvent-inaccessible NH groups generally exchange very slowly. H−D footprinting experiments with LTC_4 were attempted to resolve this issue. However, since MGST1 binds a single molecule of LTC_4 per trimer, the footprinting experiments were unsuccessful (data not shown).

DISCUSSION

Interpretation of H−D Exchange Data in the Context of the Crystal Structure. The H−D exchange kinetic results presented here were obtained in detergent solution under conditions where most of the biochemical experiments on the purified enzyme have been performed. In contrast, the structural data were derived from two-dimensional crystals in the presence of phospholipids. So, it is fair to ask if the two environments are sufficiently different to compromise a comparison between the H−D exchange kinetics and the crystal structure. In this regard, we have previously reported a comparison of the H−D exchange kinetics obtained from two-dimensional crystals to those obtained with the detergent complex (*13*). The detergent-solubilized MGST1·GSH and phospholipid MGST1·GSH complexes exhibit very similar H−D exchange profiles.

Examination of the Predicted GSH Binding Site. In the absence of a high-resolution structure of MGST1, or any MAPEG family member for that matter, the amide H−D exchange mass spectrometry experiments presented here provide additional structural insight into substrate and product binding by MGST1. These data localize the GSH binding site to residues within peptides 29−34, 62−69, 67−76, 75−90, and 107−120 (Figure 5A,B). These data are consistent with the 3.2 Å resolution structural model of the trimeric MGST1·GSH complex. In this model, GSH is surrounded by several potential hydrogen bonding partners (Figure 5C), including R73, E80, and Y120 from one monomer and R37′, R72′, and H75′ from an adjacent monomer (*7*). Moreover, H−D exchange studies indicate that one or more functional groups within peptide 62−69 may be involved in specifically stabilizing GS^- in the active site. Most of the residues within peptide 62−69 form part of a conserved motif, ^{63}(RTDEKV)-ERVRRA^{74} (Figure 1). This region is thought to be involved in the binding of GSH by other MAPEG proteins (*39*) and is adjacent to GSH in the structural model (*7*). However, some discrepancy does exist between the crystallographic model and the H−D exchange results presented here. The structural model does not orient the thiolate anion near residues 62−69, but instead toward R73 of one monomer. Within peptide 62−69, the closest residue to GSH is E69 (4.8 Å), the side chain of which points in the direction of the γ-Glu end of GSH. E69 is highly conserved in MAPEG family members (Figure 1) and may be involved in a hydrogen bonding network that specifically stabilizes the thiolate, GS^-.

The results of single-amino acid mutations in the predicted GSH binding site (Table 2) are consistent with both the structural model and the H−D exchange results presented here. The residues mutated are pictured in the context of the structure as shown in Figure 6. Substitution of R72′, R73 (Table 2), and H75′ (*24*) in the α2 helix leads to a somewhat lower specific activity of the enzyme toward CDNB. As shown in Figures 5C and 6, all of these residues are close to or are predicted to form hydrogen bonds to GSH in the 3.2 Å resolution structure (*7*). Other mutated residues suggested to be involved in GSH binding on the basis of H−D exchange results include N77T, E80Q, and R113K. These mutants all had very low specific activities compared to that of wild-type MGST1 (Table 2). On the basis of H−D

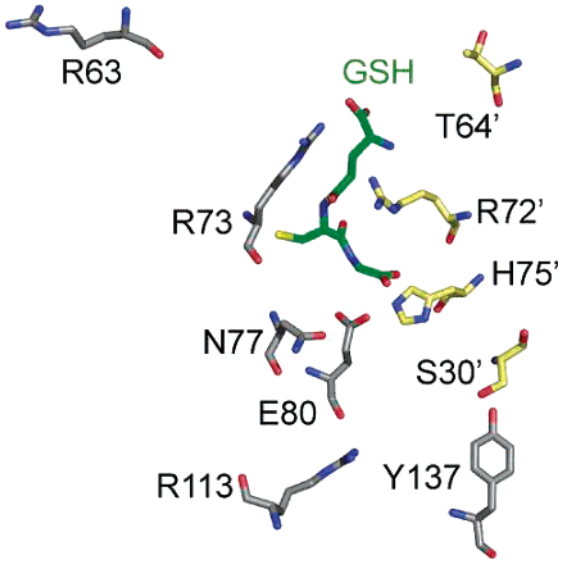

FIGURE 6: Spatial location of residues targeted for site-specific mutagenesis. Residues of MGST1 involved in the binding of GSH (green) identified by crystallography and H−D exchange footprint experiments. The specific activities of each mutation are given in Table 2. Residues from monomers A and B are indicated with gray and yellow backbone residues, respectively.

exchange, the structural model, and the mutagenesis results, it appears that residues within α-helices 1, 2, and 3 along with a small segment of the cytosolic domain come together to form the functional GSH binding site.

Examination of the Predicted Electrophilic Substrate Binding Site. The location of the electrophilic substrate binding site was probed with the product GSDNB, which should occupy both the GSH and hydrophobic binding sites (*40*, *41*). Binding at the hydrophobic site can be differentiated from binding at the GSH site through peptides that show additional decreases in the level of deuterium incorporation as a function of time when the MGST1·GSDNB complex is compared to the MGST1·GSH complex. Alternately, those peptides that retain more deuterium label in the MGST1·GSDNB complex as compared to the MGST1·GSH complex in footprinting experiments can also provide spatial information about the electrophilic substrate site. From these H−D exchange techniques, the substrate site is predicted to involve residues from peptides 44−58, 62−69, 67−76, 103−112, and 113−121 (Figure 7). It is clear that the electrophilic substrate binding site overlaps the GSH binding site to some degree but also exhibits additional contacts, a fact that is consistent with the spatial resolution of the H−D exchange experiment. These additional areas of protection from H−D exchange include residues 44−58 in the cytosolic domain connecting α1 to α2 and residues 62−69 located in the cytosolic α-helical extension of transmembrane helix α2.

It is interesting to note that part of the cytosolic domain encompassing residues 44−58 is involved in binding electrophilic substrates. This region is predicted to have a high degree of solvent exposure or to be structurally disordered in apoMGST1 based on the large amount of deuterium incorporation in 15 s (Figure 3E). The current crystallographic data for MGST1 reveal molecular density in the cytosolic domain that may be part of the connection between α1 and α2. However, at this juncture, the molecular density has not been successfully modeled, a fact that suggests

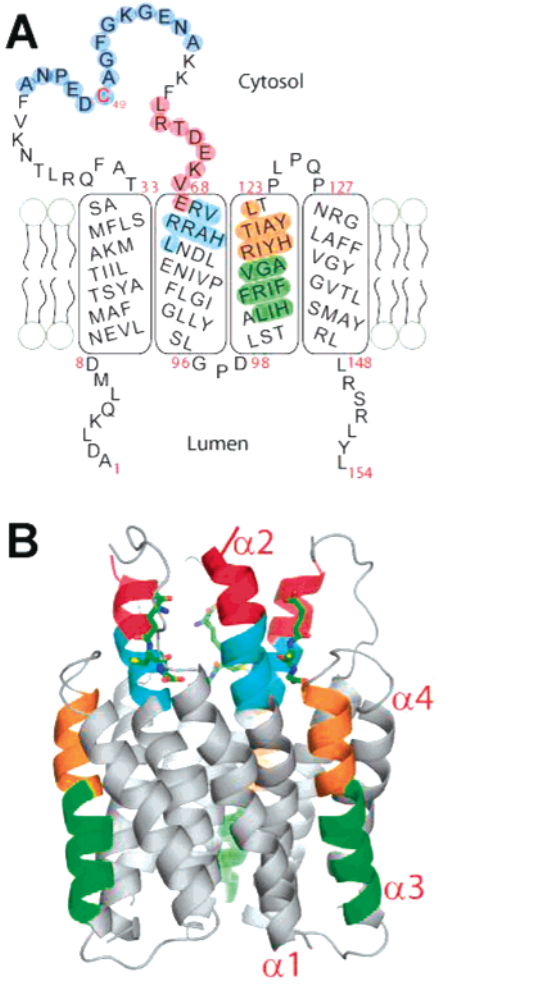

FIGURE 7: Regions involved in binding hydrophobic second substrates (blue) as indicated by amide H−D exchange kinetics and H−D footprinting with GSDNB. Peptides undergoing changes in H−D exchange are mapped to the primary sequence with lipid-embedded helices (A) and the electron crystallographic model of trimeric MGST1 (B) with the three observed GSH molecules colored green (*7*). Peptides involved in the binding of hydrophobic substrates based on H−D exchange results are colored as follows: blue for 44−58, red for 62−69, green for 103−112, and orange for 113−121. Residues from peptide 67−76 overlap other peptides; therefore, only residues 70−74 are colored cyan.

structural disorder in this region. The structure does exhibit molecular density in close contact with the loop connecting α3 and α4 of the opposing monomer (*7*). It is important to note that H−D exchange clearly demonstrates that this disordered cytosolic segment undergoes a conformational transition upon binding GSH, GSO_3^-, and GSDNB (Figure 3E). However, GSH does not protect deuterated amides within peptide 44−58 from off-exchange in footprinting experiments (data not shown). This suggests that the electrophilic substrate site undergoes reorganization in the presence of GSH to form a site more amenable to binding of the substrate. The additional protection of peptide 44−58 by the product GSDNB is consistent with the notion that the region is involved in binding electrophilic substrates. In fact, previous H−D exchange kinetic experiments with the NEM-alkylated form of apoMGST1 also displayed a significant decrease in the level of deuterium incorporation with peptide 44−58 (*13*), similar to that observed here in the MGST1·GSDNB complex. Therefore, it appears that NEM

modification of C49 may impact the structure of the substrate site in the absence of GSH and contribute to enzymatic activation by mimicking the rate-limiting conformational transition prior to the binding of GSH and the electrophilic substrate (*13*). The observation fits well with the apparent augmentation of thiolate anion formation in the presence of product and other ligands (*43*). In this scenario, product formation facilitates thiolate anion formation on a neighboring subunit by interaction with the activator site.

Examination of the Predicted Fatty Acid/Phospholipid Binding Site. Although MGST1 has glutathione-dependent fatty acid and phospholipid hydroperoxide peroxidase activity, the binding site for these specific substrates has yet to be structurally elucidated. Leukotriene C_4 is a GSH conjugate of leukotriene A_4, an epoxide derivative of arachidonic acid. Although leukotriene A_4 is not a substrate for MGST1, the product LTC_4 is a tight-binding inhibitor of GSH transferase activity (*16*). Given that LTC_4 is a glutathione adduct of a fatty acid derivative, this ligand may mimic binding at both the GSH and fatty acid/phospholipid sites.

Amide H−D exchange kinetic experiments indicate that LTC_4 is capable of producing conformational changes similar to those elicited by GSH, with the exception of cytosolic segment 44−58 and the enhanced exchange in the α1 and α3 transmembrane helices (Figure 3A,B,E). Inasmuch as MGST1 binds only one molecule of LTC_4 per trimer (*16*), the absence of changes in the kinetic profiles for H−D exchange in peptides 19−23, 104−106, and 44−58 may be due to the incomplete occupancy of the active site by the GSH moiety of the conjugate. Regardless, these data clearly show that the specific conformational change involving these two helices is not supported by the presence of GSH conjugates in the forms tested here (GSDNB and LTC_4). This conformational transition must be specific to occupation of the GSH binding site, but not the electrophilic or fatty acid binding sites. These results do suggest, however, that the fatty acid and GSH binding sites overlap to some degree since no additional changes in H−D exchange were observed in the MGST1·LTC_4 complex when compared to the MGST1·GSH complex. Consequently, the GSH site formed from residues within peptides 29−34, 62−69, 67−76, 75−90, and 107−120 may also encompass the fatty acid/phospholipid binding site. It is noteworthy that a suggested alternate membrane access to the active site does overlap with some of the residues identified as being important in the binding of LTC_4, indicating the possibility that lipid substrates could bind while still associated with the membrane. Holm et al. (*7*) postulate that highly hydrophobic substrates such as phospholipid hydroperoxides may access the fatty acid binding site through a large opening at the subunit interface of MGST1 rather than from the cytosol (*7*). The H−D exchange data presented here support this hypothesis, but clearly more investigation is required.

CONCLUSIONS

Amide hydrogen−deuterium exchange mass spectrometry has proven to be a valuable technique in providing structural information for integral membrane proteins, especially those without high-resolution three-dimensional structures. Here, the technique was utilized for an important detoxication enzyme, microsomal glutathione transferase-1, to define changes in backbone structure and dynamics that occur when substrate binding sites are occupied by their respective ligands. Identification of substrate binding sites in MGST1 can be used as the archetype for other MAPEG family members that, on the basis of homology, are all predicted to have comparable tertiary and quaternary structures and may bind substrate ligands similarly (*44*).

H−D exchange kinetics and H−D ligand footprinting experiments indicate that the binding sites for GSH and electrophilic substrates are localized within similar, but distinct, regions of MGST1. By in vitro mutagenesis, the location of the GSH binding site was experimentally tested. Those results support both structural and H−D exchange data for the location of the GSH binding site. However, site-directed mutagenesis has yet to identify a specific residue that participates in lowering the pK_a of GSH, perhaps indicating that more than one residue or a main chain functional group may be required for deprotonation of the thiol. Additionally, residues that surround the chemical stress sensor C49 appear to play an important role in the formation of the hydrophobic substrate site. Experiments utilizing leukotriene C_4 suggest that the fatty acid/phospholipid binding site of MGST1 overlaps the GSH binding site but is distinct from the hydrophobic site. Furthermore, the data presented here with GSH and the product GSDNB demonstrate that two transmembrane α-helices in MGST1 (α1 and α3) participate in conformational changes that are involved in substrate binding and product release. These experiments provide insight into the structure and function of MGST1 and highlight specific regions of the protein for further mechanistic exploration.

ACKNOWLEDGMENT

We thank the Mass Spectrometry Research Core, Center in Molecular Toxicology at Vanderbilt University School of Medicine, for the use of the mass spectrometers and for help with the instrumentation.

SUPPORTING INFORMATION AVAILABLE

Parameters for the fits to the kinetic profiles in Figure 3 (Table S1). This material is available free of charge via the Internet at http://pubs.acs.org.

REFERENCES

1. Jakobsson, P. J., Morgenstern, R., Mancini, J., Ford-Hutchinson, A., and Persson, B. (1999) Common structural features of MAPEG: A widespread superfamily of membrane associated proteins with highly divergent functions in eicosanoid and glutathione metabolism, *Protein Sci. 8*, 689−692.
2. Jakobsson, P. J., Morgenstern, R., Mancini, J., Ford-Hutchinson, A., and Persson, B. (2000) Membrane-associated proteins in eicosanoid and glutathione metabolism (MAPEG). A widespread protein superfamily, *Am. J. Respir. Crit. Care Med. 161*, S20−S24.
3. Johansson, K., Åhlen, K., Rinaldi, R., Sahlander, K., Siritantikorn, A., and Morgenstern, R. (2006) Microsomal glutathione transferase 1 in anti-cancer drug resistance, *Carcinogenesis* (in press).
4. Andersson, C., Mosialou, E., Weinander, R., and Morgenstern, R. (1994) Enzymology of microsomal glutathione S-transferase, *Adv. Pharmacol. 27*, 19−35.
5. Mosialou, E., Ekström, G., Adang, A. E., and Morgenstern, R. (1993) Evidence that rat liver microsomal glutathione transferase is responsible for glutathione-dependent protection against lipid peroxidation, *Biochem. Pharmacol. 45*, 1645−1651.
6. Mosialou, E., Piemonte, F., Andersson, C., Vos, R. M., van Bladeren, P. J., and Morgenstern, R. (1995) Microsomal glutathione transferase: Lipid-derived substrates and lipid dependence, *Arch. Biochem. Biophys. 320*, 210−216.

7. Holm, P. J., Bhakat, P., Jegerschold, C., Gyobu, N., Mitsuoka, K., Fujiyoshi, Y., Morgenstern, R., and Hebert, H. (2006) Structural basis for detoxification and oxidative stress protection in membranes, *J. Mol. Biol. 360*, 934−945.
8. Holm, P. J., Morgenstern, R., and Hebert, H. (2002) The 3-D structure of microsomal glutathione transferase 1 at 6 Å resolution as determined by electron crystallography of p22(1)2(1) crystals, *Biochim. Biophys. Acta 1594*, 276−285.
9. Morgenstern, R., Lundqvist, G., Hancock, V., and DePierre, J. W. (1988) Studies on the activity and activation of rat liver microsomal glutathione transferase, in particular with a substrate analogue series, *J. Biol. Chem. 263*, 6671−6675.
10. Morgenstern, R., Lundquist, G., Jörnvall, H., and DePierre, J. W. (1989) Activation of rat liver microsomal glutathione transferase by limited proteolysis, *Biochem. J. 260*, 577−582.
11. Svensson, R., Rinaldi, R., Swedmark, S., and Morgenstern, R. (2000) Reactivity of cysteine-49 and its influence on the activation of microsomal glutathione transferase 1: Evidence for subunit interaction, *Biochemistry 39*, 15144−15149.
12. Svensson, R., Ålander, J., Armstrong, R. N., and Morgenstern, R. (2004) Kinetic characterization of thiolate anion formation and chemical catalysis of activated microsomal glutathione transferase 1, *Biochemistry 43*, 8869−8877.
13. Busenlehner, L. S., Codreanu, S. G., Holm, P. J., Bhakat, P., Hebert, H., Morgenstern, R., and Armstrong, R. N. (2004) Stress sensor triggers conformational response of the integral membrane protein MGST1, *Biochemistry 43*, 11145−11152.
14. Morgenstern, R., Svensson, R., Bernat, B. A., and Armstrong, R. N. (2001) Kinetic analysis of the slow ionization of glutathione by microsomal glutathione transferase MGST1, *Biochemistry 40*, 3378−3384.
15. Morgenstern, R. (1998) A simple alternate substrate test can help determine the aqueous or bilayer location of binding sites for hydrophobic ligands/substrates on membrane proteins, *Chem. Res. Toxicol. 11*, 703−707.
16. Bannenberg, G., Dahlén, S. E., Luijerink, M., Lundqvist, G., and Morgenstern, R. (1999) Leukotriene C4 is a tight-binding inhibitor of microsomal glutathione transferase-1. Effects of leukotriene pathway modifiers, *J. Biol. Chem. 274*, 1994−1999.
17. Metters, K. M., Sawyer, N., and Nicholson, D. W. (1994) Microsomal glutathione S-transferase is the predominant leukotriene C4 binding site in cellular membranes, *J. Biol. Chem. 269*, 12816−12823.
18. Söderström, M., Morgenstern, R., and Hammarström, S. (1995) Protein-protein interaction affinity chromatography of leukotriene C4 synthase, *Protein Expression Purif. 6*, 352−356.
19. Surapureddi, S., Morgenstern, R., Söderström, M., and Hammarström, S. (1996) Interaction of human leukotriene C4 synthase and microsomal glutathione transferase in vivo, *Biochem. Biophys. Res. Commun. 229*, 388−395.
20. Surapureddi, S., Svartz, J., Magnusson, K. E., Hammarström, S., and Söderström, M. (2000) Colocalization of leukotriene C synthase and microsomal glutathione S-transferase elucidated by indirect immunofluorescence analysis, *FEBS Lett. 480*, 239−243.
21. Morgenstern, R., Guthenberg, C., and DePierre, J. W. (1982) Microsomal glutathione S-transferase. Purification, initial characterization and demonstration that it is not identical to the cytosolic glutathione S-transferases A, B and C, *Eur. J. Biochem. 128*, 243−248.
22. Weinander, R., Mosialou, E., DeJong, J., Tu, C. P., Dypbukt, J., Bergman, T., Barnes, H. J., Hoog, J. O., and Morgenstern, R. (1995) Heterologous expression of rat liver microsomal glutathione transferase in simian COS cells and *Escherichia coli*, *Biochem. J. 311*, 861−866.
23. Peterson, G. L. (1977) A simplification of the protein assay method of Lowry et al. which is more generally applicable, *Anal. Biochem. 83*, 346−356.
24. Weinander, R., Ekström, L., Andersson, C., Raza, H., Bergman, T., and Morgenstern, R. (1997) Structural and functional aspects of rat microsomal glutathione transferase. The roles of cysteine 49, arginine 107, lysine 67, histidine, and tyrosine residues, *J. Biol. Chem. 272*, 8871−8877.
25. Chang, G. G., Tsai, L. N., Tang, S. S., and Wang, T. C. (1994) Purification and kinetic mechanism of the glutathione S-transferase from C6/36, an *Aedes albopictus* cell line, *Arch. Biochem. Biophys. 310*, 134−143.
26. Hinchman, C. A., Matsumoto, H., Simmons, T. W., and Ballatori, N. (1991) Intrahepatic conversion of a glutathione conjugate to its mercapturic acid. Metabolism of 1-chloro-2,4-dinitrobenzene in isolated perfused rat and guinea pig livers, *J. Biol. Chem. 266*, 22179−22185.
27. Busenlehner, L. S., and Armstrong, R. N. (2005) Insights into enzyme structure and dynamics elucidated by amide H/D exchange mass spectrometry, *Arch. Biochem. Biophys. 433*, 34−46.
28. Zhang, Z., and Marshall, A. G. (1998) A universal algorithm for fast and automated charge state deconvolution of electrospray mass-to-charge ratio spectra, *J. Am. Soc. Mass Spectrom. 9*, 225−233.
29. Zhang, Z., and Smith, D. L. (1993) Determination of amide hydrogen exchange by mass spectrometry: A new tool for protein structure elucidation, *Protein Sci. 2*, 522−531.
30. Mandell, J. G., Falick, A. M., and Komives, E. A. (1998) Identification of protein-protein interfaces by decreased amide proton solvent accessibility, *Proc. Natl. Acad. Sci. U.S.A. 95*, 14705−14710.
31. Xiao, H., Kaltashov, I. A., and Eyles, S. J. (2003) Indirect assessment of small hydrophobic ligand binding to a model protein using a combination of ESI MS and HDX/ESI MS, *J. Am. Soc. Mass Spectrom. 14*, 506−515.
32. Hoofnagle, A. N., Resing, K. A., and Ahn, N. G. (2004) Practical methods for deuterium exchange/mass spectrometry, *Methods Mol. Biol. 250*, 283−298.
33. Sun, T. H., and Morgenstern, R. (1997) Binding of glutathione and an inhibitor to microsomal glutathione transferase, *Biochem. J. 326*, 193−196.
34. Lengqvist, J., Svensson, R., Evergren, E., Morgenstern, R., and Griffiths, W. J. (2004) Observation of an intact noncovalent homotrimer of detergent-solubilized rat microsomal glutathione transferase-1 by electrospray mass spectrometry, *J. Biol. Chem. 279*, 13311−13316.
35. Codreanu, S. G., Thompson, L. C., Hachey, D. L., Dirr, H. W., and Armstrong, R. N. (2005) Influence of the dimer interface on glutathione transferase structure and dynamics revealed by amide H/D exchange spectrometry, *Biochemistry 44*, 10605−10612.
36. Grahn, E., Novotny, M., Jakobsson, E., Gustafsson, A., Grehn, L., Olin, B., Madsen, D., Wahlberg, M., Mannervik, B., and Klevwegt, G. J. (2006) New crystal structures of human glutathione transferase a1-1 shed light on glutathione binding and the conformation of the C-terminal helix, *Acta Crystallogr. D62*, 197−207.
37. Gracia, R. A., Pantazatos, D., and Villarreal, F. J. (2004) Hydrogen/deuterium exchange mass spectrometry for investigating protein-ligand interactions, *Assay Drug Dev. Technol. 2*, 81−91.
38. Morgenstern, R., DePierre, J. W., and Jörnvall, H. (1985) Microsomal glutathione transferase. Primary structure, *J. Biol. Chem. 260*, 13976−13983.
39. Bresell, A., Weinander, R., Lundqvist, G., Raza, H., Shimoji, M., Sun, T. H., Balk, L., Wiklund, R., Eriksson, J., Jansson, C., Persson, B., Jakobsson, P. J., and Morgenstern, R. (2005) Bioinformatic and enzymatic characterization of the MAPEG superfamily, *FEBS Lett. 272*, 1688−1703.
40. Cardoso, R. M., Daniels, D. S., Bruns, C. M., and Tainer, J. A. (2003) Characterization of the electrophile binding site and substrate binding mode of the 26-kDa glutathione S-transferase from *Schistosoma japonicum*, *Proteins 51*, 137−146.
41. Reinemer, P., Dirr, H. W., Ladenstein, R., Huber, R., Lo Bello, M., Federici, G., and Parker, M. W. (1992) Three-dimensional structure of class pi glutathione S-transferase from human placenta in complex with S-hexylglutathione at 2.8 Å resolution, *J. Mol. Biol. 227*, 214−226.
42. Murakami, M., Naraba, H., Tanioka, T., Semmyo, N., Nakatani, Y., Kojima, F., Ikeda, T., Fueki, M., Ueno, A., Oh, S., and Kudo, I. (2000) Regulation of prostaglandin E2 biosynthesis by inducible membrane-associated prostaglandin E2 synthase that acts in concert with cyclooxygenase-2, *J. Biol. Chem. 275*, 32783−32792.
43. Mosialou, E., and Morgenstern, R. (1990) Inhibition studies on rat liver microsomal glutathione transferase, *Chem.-Biol. Interact. 74*, 275−280.
44. Hebert, H., Jegerschold, C., Bhakat, P., and Holm, P. J. (2005) Two-dimensional crystallization and electron crystallography of MAPEG proteins, *Methods Enzymol. 401*, 161−168.
45. Thompson, J. D., Higgins, D. G., and Gibson, T. J. (1994) CLUSTAL W: Improving the sensitivity of progressive multiple sequence alignment through sequence weighting, position-specific gap penalties and weight matrix choice, *Nucleic Acids Res. 22*, 4673−4680.

BI6023385